The Cryosphere Discuss., 3, 947–993, 2009
www.the-cryosphere-discuss.net/3/947/2009/

The Cryosphere Discussions

This discussion paper is/has been under review for the journal The Cryosphere (TC).
Please refer to the corresponding final paper in TC if available.

Response of the ice cap Hardangerjøkulen in southern Norway to the 20th and 21st century climates

R. H. Giesen and J. Oerlemans

Institute for Marine and Atmospheric research Utrecht, Utrecht University, P.O. Box 80005, 3508 TA Utrecht, The Netherlands

Received: 27 October 2009 – Accepted: 2 November 2009 – Published: 13 November 2009

Correspondence to: R. H. Giesen (r.h.giesen@uu.nl)

Published by Copernicus Publications on behalf of the European Geosciences Union.

Abstract

Glacier mass balance changes lead to geometry changes and vice versa. To include this interdependence in the response of glaciers to climate change, models should include an interactive scheme coupling mass balance and ice dynamics. In this study, we couple a spatially distributed mass balance model to a two-dimensional ice-flow model and apply this coupled model to the ice cap Hardangerjøkulen in southern Norway. The available glacio-meteorological records, mass balance and glacier length change measurements were utilized for model calibration and validation. Driven with meteorological data from nearby synoptic weather stations, the coupled model realistically simulated the observed mass balance and glacier length changes during the 20th century. The mean climate for the period 1961–1990, computed from local meteorological data, was used as a basis to prescribe climate projections for the 21st century at Hardangerjøkulen. For a projected temperature increase of 3°C from 1961–1990 to 2071–2100, the modelled net mass balance soon becomes negative at all altitudes and Hardangerjøkulen disappears around the year 2100. The projected changes in the other meteorological variables could at most partly compensate for the effect of the projected warming.

1 Introduction

Glacier volume projections are required to assess the rate of sea level rise expected from ice wastage in a warmer future climate (e.g., IPCC, 2007; Meier et al., 2007; Bahr et al., 2009). In order to obtain reliable estimates for a particular climate scenario, observed differences in glacier response for various glacier types and climatic regions first need to be understood.

In contrast to most other regions in Scandinavia and the global trend, the maritime glaciers in mainland Norway advanced in the late 20th century, following a series of wet winters around 1990 (Andreassen et al., 2005). Since the year 2000, all monitored

glaciers in Norway had a net mass deficit and retreated (Kjøllmoen et al., 2008). On the maritime Norwegian glaciers, the interannual variability in the net mass balance is dominated by variations in the winter balance, while summer balance fluctuations are more important on the glaciers further inland (Andreassen et al., 2005). The high dependence on winter precipitation suggests that the future of the maritime Norwegian glaciers is not only determined by the degree of warming, but also by the accompanying change in precipitation.

Regarding the spatial distribution of glaciers in southern Norway, the large glaciers (>25 km^2) are all situated relatively close to the coast, in a rather maritime regime. All these glaciers are ice caps, with a large and flat upper part and a number of steeper outlet glaciers. Ice caps are particularly sensitive to climate change, because a small increase in the equilibrium-line altitude (ELA) can turn a large part of the accumulation area into ablation area (Nesje et al., 2008).

In this study, we determine the response of the ice cap Hardangerjøkulen in southern Norway to the observed climate in the 20th century and projected climate change for the 21st century. Hardangerjøkulen is situated in the transitional zone between the maritime glaciers near the western coast and the more continental glaciers further inland (Andreassen et al., 2005; Giesen et al., 2009). We employ a spatially distributed surface mass balance model coupled to a two-dimensional (2-D) ice-flow model to assess the effect of climate fluctuations on Hardangerjøkulen. By using a spatially distributed mass balance model, we can take into account horizontal precipitation gradients and topographic effects, especially on solar irradiance. All individual energy and mass balance fluxes are defined as functions of principal meteorological variables, which is essential to translate changes in climate to a change in surface mass balance. Simple relations, for instance between air temperature and ablation, may no longer be valid in a climate that is much warmer than the climate used to calibrate the relationship. Compared to lower-order models, 2-D ice-flow models have no restrictions regarding the spatial distribution of ice; the glacier geometry keeps adapting to changes in the mass balance. This is especially important for ice caps like Hardangerjøkulen, with

multiple drainage basins and ice flow in all directions. Since geometry changes are dictated by mass changes, but in return affect the surface mass balance, the mass balance and ice-flow models need to be coupled on a time-scale much shorter than the response time of the ice cap. By coupling the two models annually, we include the feedback mechanisms associated with this interdependence.

The main objective of this paper is to provide simulations of the future evolution of Hardangerjøkulen for a range of climate projections. First, we describe the model and the meteorological records used to drive the model. We then compare the modelled and measured energy and mass balance fluxes and demonstrate that the model can reproduce the observed ice cap geometry through the 20th century. We discuss the ice cap volume change for different 21st century climate projections and show the simulated ice cap geometry for one of the most probable climate changes in more detail. Furthermore, we investigate the role of feedback processes in our ice cap simulations.

2 Hardangerjøkulen

The ice cap Hardangerjøkulen (60.55°N, 7.43°E) is situated in southern Norway, 150 km from the western coast (Fig. 1). The present-day ice cap covers 73 km^2 and ranges in altitude from 1020 to 1865 m a.s.l. (Fig. 2).

Annual winter, summer and net mass balances have been measured on the largest, westerly draining outlet glacier Rembesdalsskåka since 1963. The winter balance is usually determined in May, the summer and net balance in early October (Andreassen et al., 2005). The mean net mass balance over the period 1963–2005 was slightly positive (+0.13 m water equivalent [w.e.]), with a mean winter balance of +2.11 m w.e. and a mean summer balance of −1.98 m w.e. (Kjøllmoen et al., 2006). Based on the mean net mass balance profile for Rembesdalsskåka over the 33 profiles measured between 1965 and 2005, 80% of the total area of Rembesdalsskåka is located above the mean ELA (1640 m a.s.l.).

Since October 2000, an automatic weather station (AWS) is operating in the ablation

TCD
3, 947–993, 2009

zone (1450 m a.s.l.) of the north-easterly outlet glacier Midtdalsbreen, providing all meteorological quantities needed to calculate the local surface energy balance (Giesen et al., 2008). This station was supplemented by a second AWS on the summit of Hardangerjøkulen (1860 m a.s.l.), which was in operation during the summer of 2005.

Glacier length has been measured at Rembesdalsskåka during several intervals, the first measurement dating from 1917. At Midtdalsbreen, glacier length has been measured annually since 1982 (Andreassen et al., 2005). The length measurements were combined with maps and dated moraines in the glacier forefields to reconstruct glacier length records for the 20th century, used for validation of the coupled model (data provided by H. Elvehøy, NVE, Oslo).

The last major advance of Hardangerjøkulen occurred around AD 1750, in the "Little Ice Age" (LIA). During this advance, almost all older moraines were overridden. Figure 2 shows the LIA extent for the north-eastern and south-western parts of Hardangerjøkulen, determined from terminal moraines (Andersen and Sollid, 1971; Nesje and Dahl, 1991; Nesje et al., 1994; Elvehøy et al., 1997). At some locations around the ice cap, pre-LIA marginal moraines, deposited around 10 000 years before present (BP), are found just outside the LIA moraines (Nesje and Dahl, 1991). The history of Hardangerjøkulen between these two major advances was reconstructed from a series of terrestrial stratigraphic sections and lake sediment cores at the north-eastern side of the ice cap and one sediment core from the south-western side (Dahl and Nesje, 1994; Nesje et al., 1994). These studies indicate that another large advance occurred around 8300 BP, probably related to the wide-spread cold event around 8200 BP (e.g. Alley et al., 1997). Between roughly 7000 and 4000 BP, several periods without any deposition of glacial sediments occurred, indicating that no glaciers were present in the catchment. During this period, summer air temperatures in southern Norway were approximately 1.5–2.0°C higher than at present (Bjune et al., 2005) and all investigated glaciers in Norway disappeared (Nesje et al., 2008). From 4000 BP until the present, Hardangerjøkulen existed continuously and had probably grown to its present-day extent by 1000 BP. Since the LIA maximum Rembesdalsskåka has retreated almost two

kilometres, while Midtdalsbreen retreated approximately one kilometre (Andersen and Sollid, 1971; Elvehøy et al., 1997, Fig. 2).

3 Model description

3.1 Ice-flow model

We employ an ice-flow model that was previously used to simulate the Eurasian ice sheet through the last glacial cycle (Van den Berg et al., 2008). The model is based on the vertically integrated continuity equation and uses the shallow-ice approximation (SIA; e.g. Hutter, 1983). Since we are interested in the response of the ice cap to mass balance changes over decadal time-scales and the surface and bedrock slopes of Hardangerjøkulen are generally gentle, the SIA can be expected to produce reasonably accurate results (Leysinger Vieli and Gudmundsson, 2004). The vertical mean horizontal velocity is divided into contributions by internal deformation and basal sliding, including constant deformation and sliding parameters, respectively. These two model parameters were optimized for Hardangerjøkulen by means of a dynamic calibration (Oerlemans, 1997) with the observed length changes at Rembesdalsskåka and Midtdalsbreen (Giesen, 2009, Ch. 6). All spatial derivatives are calculated with central differencing, for the time integration an Alternating Direction Implicit (ADI) method is used (e.g. Huybrechts, 1992). We use a time-step of 0.01 year, which is sufficiently small to exclude numerical instabilities.

3.2 Mass balance model

The mass balance model only includes mass changes at the surface of the ice cap, basal melting and calving at the glacier front are not included. Currently, the largest outlet glaciers of Hardangerjøkulen do not terminate in water, but Rembesdalsskåka did end in the lake Rembesdalsvatnet when the ice cap was larger (Fig. 2; Elvehøy

et al., 1997). Basal melt is assumed to be small compared to the high ablation rates at the ice cap surface.

The surface mass balance model is based on a model developed for Morteratschgletscher in Switzerland (Klok and Oerlemans, 2002). Thorough calibration of the model parameterizations was needed before the model could be applied at Hardangerjøkulen, where climatic conditions are different. Based on the AWS data from Midtdalsbreen, adjustments were made to the parameterizations for the surface albedo and the turbulent fluxes. Below we give a summary of the main model characteristics, for details of the calibration procedure and the values used for the model parameters, we refer to Giesen (2009), Ch. 5.

The annual surface mass balance B (mw.e.) at each location in the model domain is determined by three processes

$$B = \int_{\text{year}} \left[P_{\text{snow}} - M - S \right] \, dt, \tag{1}$$

where P_{snow} is the amount of solid precipitation, M is the mass removed by ablation at the surface and S represents mass exchange with the air by sublimation or rime. The surface mass balance is calculated using a time-step of 60 min.

The energy available for melting Q (Wm^{-2}), is calculated from the surface energy balance:

$$Q - G = S_{\text{in}} + S_{\text{out}} + L_{\text{in}} + L_{\text{out}} + H_{\text{sen}} + H_{\text{lat}}. \tag{2}$$

S_{in} and S_{out} are incoming and reflected solar radiation, L_{in} and L_{out} are incoming and outgoing longwave radiation, H_{sen} and H_{lat} are the sensible and latent heat fluxes and G is the subsurface heat flux. Heat supplied by rain is neglected, which is justified on glaciers with a considerable mass turnover (Oerlemans, 2001). Fluxes directed towards the surface are defined positive. When the sum of the fluxes on the right-hand-side of Eq. (2) is positive, this energy is first used to heat the surface to the

melting point; remaining energy is used to melt snow or ice. The amount of melt M (mw.e.) is calculated from the melting energy Q:

$$M = \frac{Q}{L_f \rho_w}. \quad (3)$$

with L_f the latent heat of fusion ($3.34 \times 10^5\,\mathrm{J\,kg^{-1}}$) and ρ_w the density of water ($1000\,\mathrm{kg\,m^{-3}}$). Sublimation ($S$) is determined from the latent heat flux

$$S = -\frac{H_{lat}}{L_s \rho_w}. \quad (4)$$

where L_s ($2.83 \times 10^6\,\mathrm{J\,kg^{-1}}$) is the latent heat of sublimation. The model only keeps track of changes in solid mass. When the surface is at the melting point, we assume there is meltwater available for vaporization.

Refreezing of rain and meltwater in the snowpack is not included in the model, although ice formation has been observed in Hardangerjøkulen's accumulation area (Laumann, 1972). The available measurements are insufficient to determine the net effect of refreezing on the mass balance. Considering that substantial ablation occurs even at the highest altitudes (1–2 mw.e. according to the mass balance measurements), the amount of energy needed to heat the snowpack to the melting temperature is much smaller than the total energy available during the summer season.

The mass balance model computes the individual fluxes of the surface energy and mass balance at each grid cell, based on sub-daily records of air temperature, relative humidity, air pressure and cloudiness and daily precipitation. A seasonally varying lapse rate is used to extrapolate measured air temperatures to the altitude of the AWS on Midtdalsbreen (Sect. A3), a constant lapse rate ($6.5\,\mathrm{K\,km^{-1}}$) is used for subsequent extrapolation over the ice cap. Measured relative humidity is converted to water vapour pressure, for both water vapour and air pressure an exponential decrease with altitude is assumed. We assume that the observed cloud fraction is valid for the entire model domain. Precipitation is distributed over the ice cap according to the

altitudinal profile measured on Rembesdalsskåka, giving a general precipitation increase with altitude, but a decrease above 1800 m a.s.l. To simulate the effect of the predominant (south)westerly flow on the precipitation distribution, we impose a linear south-west–north-east precipitation gradient over the model domain, with higher values in the south-west. The effect of the surface orientation is taken into account in the calculations of the incoming solar radiation. The surface albedo of snow is a function of air temperature during snowfall, time since the last snowfall and snow depth. When the snow has melted, we use constant albedo values for ice (0.35) and bare rock (0.15). Incoming longwave radiation is a function of air temperature, humidity and cloudiness, the outgoing longwave radiation is calculated from the surface temperature, determined from a three-layer subsurface model. The turbulent fluxes are determined with the bulk method, where we prescribe a seasonally varying turbulent exchange coefficient that is dependent on cloudiness. Based on a comparison with measured ablation, we prescribe a larger turbulent exchange coefficient on the ice cap plateau (above 1650 m a.s.l.).

3.3 The coupled model

All calculations are performed on a $18 \times 18\,\mathrm{km}^2$ model domain with a horizontal resolution of 100 m. For the present-day surface topography, we use a digital elevation model (DEM) for Hardangerjøkulen created by the Norwegian Mapping Authority (Statens Kartverk), based on aerial photographs from 1995. Model years are shifted with respect to calendar years and run from 1 October in the previous year to 30 September in the corresponding calendar year. In this way, a model year approximates one mass balance year, consisting of an accumulation season and the following ablation season. Since we use constant deformation and sliding parameters in the ice-flow model, seasonal variations in the ice flow cannot be modelled. This is not a problem, because we are only interested in the long-term evolution of Hardangerjøkulen. For the same reason, it is not necessary to couple the models at sub-annual time-scales. We therefore compute the annual surface mass balance on a fixed grid and supply the resulting

mass balance field to the ice-flow model to compute the ice thickness changes induces by the annual mass balance. The updated surface topography and ice cap extent are returned to the mass balance model to start the calculations for the next year. At the beginning of each mass balance year, new surface slope, aspect and horizon angles are computed from the updated surface topography and used in the radiation calculations. We assume that the typical shape of the altitudinal precipitation profile is primarily resulting from the plateau geometry and less from its absolute elevation. We therefore let the maximum in the precipitation profile change along with variations in the summit elevation. In the same way, the altitude above which we prescribe an increase in the turbulent exchange coefficient (1650 m a.s.l. for the present-day geometry) is adjusted when the summit elevation changes.

4 Meteorological input data

4.1 Observational records

For the 20th century, the model is driven with meteorological observations of air temperature, relative humidity, air pressure, cloudiness and precipitation. From 1957 onwards, these are available from stations in the vicinity of Hardangerjøkulen, for earlier years we use data from Bergen (Fig. 1), combined with simple parameterizations for air pressure and cloudiness. A description of the records and their implementation in the model is given in the appendix.

4.2 Control climate (1961–1990)

The future climate is simulated by a superposition of climatological data and linear changes in the meteorological variables from 1961–1990 to 2071–2100. Local meteorological data for the period 1961–1990 form the basis for the climatological control series (Sect. A1). The climatological annual cycle was simply defined as the 30 year

average for each daily or hourly interval as used in the model (Fig. 3). Air temperature has a sinusoidal seasonal cycle with a minimum in early February and a maximum in early August. The annual temperature range is 18°C, similar to the annual range in the AWS measurements from Midtdalsbreen (Giesen et al., 2008). Daily mean relative humidity is higher than 70% through the year, with the lowest values in early June. Cloudiness and precipitation show a similar annual cycle with maximum values in autumn and minimum values in late spring and early summer. The mean summer temperature for 1961–1990 is about 1°C lower than during the AWS period (2001–2005), while winter precipitation was approximately 15% lower.

4.3 The RegClim projections

To model future mass balances, we apply climate projections for southern Norway from the RegClim project (http://regclim.met.no). The projected changes in temperature and precipitation depend on the choice of the emission scenario, the climate model and the downscaling method. We therefore use a number of different projections as input to the model, to determine the variability in the ice cap response to different climate changes. The climate projections give the change in air temperature, precipitation, cloudiness, air pressure and wind speed from the normal period 1961–1990 to 2071–2100. For the area around Hardangerjøkulen, the RegClim results indicate an increase in the annual mean temperature (ΔT) of approximately 3°C from 1961–1990 to 2071–2100, with the largest changes in autumn and winter. Annual precipitation will probably increase by approximately 10%, although an increase of $\Delta P = 70\%$ is projected by one of the models (Räisänen et al., 2004). The projected increase in autumn and winter precipitation is larger than the annual mean change, while summer precipitation may decrease. Since the net mass balance on Hardangerjøkulen is probably more sensitive to temperature changes in summer and precipitation changes in winter, we investigate the effect of a seasonal cycle in the climate projections compared to annual changes. The projected air pressure change is smaller than ±5 hPa, which is too small to have a notable effect on the calculated mass balance and is therefore not further

investigated. Cloudiness is projected to change by less than 5% in all seasons. For present-day conditions, the effect of cloud changes on solar radiation is approximately compensated by a change in longwave radiation of the opposite sign. In a warmer climate, the balance between incoming longwave and solar radiation may change and the effect of cloud fraction changes may be different. The effect of a 5% increase in the cloud fraction in combination with a temperature increase will therefore be investigated. The projected wind speed change is within ±6%, but the effect of such a change cannot be determined easily because wind speed is only indirectly incorporated in the turbulent exchange coefficient. By increasing the turbulent exchange coefficient by 10% along with a temperature increase, we use the model to obtain a rough estimate of wind speed changes on the surface mass balance.

4.4 Climate projections in the model

All investigated future climate projections were incorporated in the same way in the model. Since the projections are defined as the change from the normal period 1961–1990 to 2071–2100, we assume a linear increase/decrease of the considered meteorological variable by the projected amount from the middle of the first period (1976) to the middle of the second period (2086). As meteorological measurements are available until 2005, the climatological data is used from 2006 onwards. Hence, the imposed climate change is already larger than zero at the beginning of the future simulation (2006). We determined the effect of various changes in annual temperature, as well as the combination of the most probable temperature increase (3°C) with different increases in precipitation. The largest increase in both temperature and precipitation is projected for autumn and winter, but the timing of the maximum and minimum is uncertain. We therefore determined the effect of a sinusoidal variation with the maximum in mid-autumn (15 October) and the minimum in mid-spring, as well as a sinusoidal variation with the maximum in mid-winter (15 January) and the minimum in mid-summer. The amplitude of the oscillation is estimated from the RegClim results, where air temperature is varied by ±0.6°C from a mean value of +3.0°C and precipitation is varied

by ±15% from a mean change of +10%.

5 Results

In order to simulate the ice cap response to future climate projections, the effect of the present-day climate on the surface energy and mass balance should be well represented in the model. Therefore, we first compare the modelled surface energy and mass balances with the AWS measurements on Midtdalsbreen and the mass balance measurements on Rembesdalsskåka. Ice dynamical effects were excluded in these model runs by keeping the topography fixed at the 1995 DEM. Subsequently, ice dynamics are included and we show the modelled response of Hardangerjøkulen to the observed climate of the 20th century and various climate scenarios for the 21st century.

5.1 Surface energy balance at the Midtdalsbreen AWS

The seasonal cycle of the surface energy balance at the Midtdalsbreen AWS is well captured by the model (Fig. 4a). Although the parameterizations for the individual fluxes were calibrated with the AWS measurements, this was often done separately for different atmospheric conditions (e.g., cloudy, clear-sky), not necessarily constraining the integrated values. Furthermore, the calibration was performed with the meteorological values measured at the AWS, while the energy fluxes shown in Fig. 4a were calculated with local meteorological data. The model generally overestimates S_{net}, while L_{net} is too negative, which may indicate that cloud conditions at the local station are slightly different from the AWS site.

For the period 1961–1990, all modelled energy fluxes are slightly smaller than for the warm 2001–2005 period (Fig. 4b). Using the control climate instead of the local meteorological records results in higher net solar radiation in several months; for the other fluxes the differences are small.

All surface energy fluxes increase or become less negative when the air temperature

is raised by 3°C, except for G, which remains close to zero (Fig. 4c). Because the winter snowpack with a high albedo disappears earlier in spring, the maximum in S_{net} occurs earlier in the season and the largest increase in melt energy is simulated for June. The somewhat smaller increase in Q in the other summer months is mainly a result of larger turbulent fluxes and a small positive contribution by L_{net}. Besides the increase in melt energy, the melt season also becomes slightly longer. Almost no change in the surface energy fluxes is modelled in winter, because the surface temperature increases along with the air temperature, as long as it is lower than the melting point temperature. Again, there are only minor differences between the seasonal cycles modelled with the local data and the control climate.

This simulation shows how the surface energy fluxes at the Midtdalsbreen AWS are affected by an instantaneous temperature increase. For the future projection of Hardangerjøkulen, the air temperature is assumed to increase linearly in time and the ice cap surface will have lowered with respect to the DEM topography by the time the temperature has increased by 3°C. The dynamic response will thereby further amplify the effect of the warming on the surface energy balance.

5.2 Surface height at the Midtdalsbreen AWS

For all input data sets, the differences in modelled accumulation and ablation at the Midtdalsbreen AWS have been analysed separately, by first using the same (local) precipitation record in all runs and varying the set with other meteorological variables. This set, containing the air temperature, humidity, pressure and cloudiness records for a given input data set, is referred to as the "meteo" record. Similar results are obtained in the three runs (Fig. 5a), hence modelled ablation at the AWS location does not deteriorate when the AWS measurements are replaced by a different "meteo" record; provided that the differences between the AWS and "meteo" records are accounted for by a careful calibration.

The variability between the results for the different data sets increases when the combination of "meteo" and precipitation records is used (Fig. 5b). The difference with

measured snow depth is large in three of the five years, leading to the largest deviations from measured net ablation in these years. In 2003 and 2004, modelled snow depth is similar to the observed snow depth and measured net ablation is better reproduced. The modelled start of the melt season and the changes in ablation rate through the summer season agree well with the observations, again confirming that the modelled energy fluxes are realistic and the differences with observations primarily originate from differences in precipitation.

When the surface topography is not allowed to change, the accumulation and ablation modelled with the control climate are the same for all years (Fig. 5c). The comparison with measured surface height changes illustrates that the modelled start and end of the ablation season correspond well to the measurements. At the AWS location, the control climate produces surface height changes that compare best to the measurements in 2001 and 2005; in the other years the accumulation was lower and ablation higher. For a 3°C higher air temperature, the largest change occurs in the ablation season; the winter accumulation commences about 15 days later, but the temperature in the winter months remains below the threshold temperature for snow. Compared to the control climate, ice melt increases by almost 3.5 m and closely resembles the measured ablation in the warm summer of 2002 (Giesen et al., 2008).

5.3 Comparison with mass balance measurements

Modelled winter, summer and net mass balance for Rembesdalsskåka are compared with NVE measurements for all 43 individual years (Fig. 6). The overall agreement between model results and measurements is good for the input data from both local stations and Bergen. The highest correlation coefficients (r) are obtained for the winter and net balance (Table 1), the interannual variability in the summer balance appears to be more difficult to simulate with the model. The best correlation is obtained by using local input data; with Bergen input data, the winter balance is underestimated in the four wettest years. This could imply that the precipitation anomaly is larger in the surroundings of Hardangerjøkulen compared to Bergen. The mean summer balance modelled

with Bergen input data is 0.19 mw.e. larger than the measured value, resulting in a higher than observed net balance in most of the years. Considering that no cloud observations are used for the simulations with data from Bergen, the model results are remarkably close to the measured values. There is little difference between the mass balance values modelled with either a constant or a responding surface topography, suggesting that the modelled surface topography does not deviate much from the 1995 DEM. A comparison of two DEMs from 1961 and 1995 indicates that elevation changes over Rembesdalsskåka were generally smaller than +15 m (Andreassen and Elvehøy, 2001).

We already showed that simulations with the control climate give seasonal energy and mass balance variations at the AWS site on Midtdalsbreen that correspond well to the measurements, especially when considering that the period 1961–1990 was colder than 2001–2005. The control climate precipitation data were multiplied by a factor of 0.96 to match the modelled winter balance with the mean value from the NVE measurements over the period 1963–1990. The modelled summer and net mass balance were not adapted in any way and correspond well to the mean NVE values, the difference is less than ±0.01 mw.e.

5.4 Spatial distribution of the mass balance

In Fig. 7 the spatial pattern of the modelled net mass balance is shown for the present-day topography (1995 DEM), together with the local mass balance deviation from the altitudinal mean. We here show the mean values modelled with local data over the period 1961–1990; the mass balance patterns are similar for other periods or input data, only the absolute values of the mass balance differ.

The highest net mass balances are simulated for the upper ice cap with values around 1 mw.e (Fig. 7a). Mass balance values are slightly lower near the summit, a result of the prescribed decrease in precipitation at the highest altitudes. There is little spatial variation in the accumulation area compared to the outlet glaciers, where the slopes are larger. The altitudinal deviations of the net mass balance mainly reflect vari-

ations due to the surface orientation and topography (Fig. 7b). Positive anomalies are found at steep north-facing slopes, where the surface orientation results in a reduction of direct solar radiation. Negative values mainly occur on the southern outlet glaciers, where the glacier surface is oriented towards the sun. Although surface slopes on Hardangerjøkulen are gentle compared to, for instance, glaciers in the European Alps, topographic effects generate considerable spatial variability in the net mass balance. The differences can primarily be attributed to the angle of incidence for solar radiation, which varies with surface slope and aspect. Topographic shading, on the other hand, plays a minor role in the spatial pattern of the net balance as it mainly occurs at large solar zenith angles (in winter, morning and evening), when the amount of ablation is small. The precipitation gradient is less prominent in Fig. 7b, but on the plateau where slope effects are small, it is visible as generally positive anomalies in the south-west and negative anomalies in the north-eastern part of the ice cap.

5.5 Mass balance sensitivity

The changes in the surface mass balance corresponding to a 1 K change in air temperature (C_T) and a 10% change in precipitation (C_P) are often computed as a measure of a glacier's sensitivity to climate change. These static mass balance sensitivities C_T and C_P do not include ice dynamic effects and are defined as (Oerlemans, 2001):

$$C_T = \frac{\mathrm{d}B_\mathrm{n}}{\mathrm{d}T} \approx \frac{B_\mathrm{n}(T+1) - B_\mathrm{n}(T-1)}{2} \quad (5)$$

$$C_P = \frac{\mathrm{d}B_\mathrm{n}}{\mathrm{d}P} \approx \frac{B_\mathrm{n}(P+10\%) - B_\mathrm{n}(P-10\%)}{2}. \quad (6)$$

We calculated C_T and C_P for the DEM topography, using local input data for the period 1961–1990. We obtained $C_T = -0.94\,\mathrm{mw.e.K^{-1}}$ and $C_P = +0.30\,\mathrm{mw.e.(10\%)^{-1}}$ for the entire ice cap Hardangerjøkulen and $C_T = -0.92\,\mathrm{mw.e.K^{-1}}$ and $C_P = +0.31\,\mathrm{mw.e.(10\%)^{-1}}$ for Rembesdalsskåka. Especially C_T is higher than found in other

studies for Rembesdalsskåka. For example, Rasmussen and Conway (2005) obtained $C_T = -0.64 \text{mw.e.K}^{-1}$ and $C_P = +0.22 \text{mw.e.}(10\%)^{-1}$, while De Woul and Hock (2005) report $C_T = -0.66 \text{mw.e.K}^{-1}$and $C_P = +0.28 \text{mw.e.}(10\%)^{-1}$ The larger sensitivity found in this study possibly results from differences in model types; while we used a distributed energy balance approach, Rasmussen and Conway (2005) regressed measured mass balance with upper-air meteorological conditions, while De Woul and Hock (2005) applied a degree-day model to nearby weather station data. The climate sensitivity of Hardangerjøkulen, calculated with the control climate is $C_T = -0.97 \text{mw.e.K}^{-1}$ and $C_P = +0.28 \text{mw.e.}(10\%)^{-1}$, almost identical to the values for the local data. These values suggest that at least a 30% increase in precipitation is needed to compensate the effect of a 1 K temperature increase.

The mass balance sensitivity for individual months is given by the seasonal sensitivity characteristic (SSC; Oerlemans and Reichert, 2000), where temperature or precipitation are only perturbed during one month at a time. We computed the SSC for Hardangerjøkulen, again using local input data for the period 1961–1990 (Fig. 8). The largest changes in the net mass balance are obtained for a temperature change in the summer months. These are the months with the highest air temperatures, the largest surface energy fluxes and the transition from snow to ice albedos at the lower (June) to higher (August) altitudes and are therefore very sensitive to changes in the energy balance. In May and October, air temperatures are close to the threshold temperature for snow. A small shift in temperature then directly enhances or reduces snow accumulation, significantly affecting the winter balance. The mass balance sensitivity to precipitation perturbations is largest in winter, when mass balance changes are dictated by the amount of solid precipitation. The lower mass balance sensitivity to precipitation changes in February compared to the surrounding months is not resulting from the shorter length of this month; the sensitivities in Fig. 8 have been normalized to standard months of 30 days. For the period 1961–1990, the precipitation in February is clearly smaller than for the other winter months (Fig. 3).

5.6 Hardangerjøkulen in the 20th century

We now use the coupled model to simulate the ice cap evolution from 1905 to 2005. With the coupled model, the surface mass balance not only varies due to changes in climate, but also reacts to changes in the surface topography and ice cap extent induced by the mass balance history. When the coupled model is able to reproduce the length change records of Rembesdalsskåka and Midtdalsbreen and the observed surface topography and ice cap extent, we can be confident that the model is able to simulate a realistic ice cap evolution for a given future climate scenario.

Because there are no maps or outlines of Hardangerjøkulen available for the early 20th century, we use the 1904 ice cap modelled in the dynamic calibration (Giesen, 2009, Ch. 6) to prescribe the ice cap geometry at the beginning of 1905. Meteorological input data from Bergen are used until 1957, local meteorological data are used from 1958 onwards.

In 1905, the modelled margin of Hardangerjøkulen was located at an intermediate position between its maximum Little Ice Age extent and the present-day geometry (Figs. 2 and 9). The ice cap decreased in volume until 1917, followed by a number of positive mass balance years that let the ice cap volume increase almost back to its 1905 volume (Fig. 10) and geometry (Fig. 9). Rembesdalsskåka is known to have advanced about 50 m between 1919 and the late 1920s, building a distinct moraine before retreating again (Fægri, 1936). This advance is smaller than the model resolution (100 m) and is therefore not captured in the modelled length change record. The modelled frontal position of Rembesdalsskåka in 1928 corresponds well to the 1928 extent reported by Liestøl (1956). Midtdalsbreen is too large compared to the 1930 moraines identified by Andersen and Sollid (1971). After this small advance in the 1920s, a period with highly negative annual mass balances led to fast volume decrease of Hardangerjøkulen until 1950 and an accelerated retreat of the outlet glaciers (Fig. 10). The net mass balance was less negative from 1949 onwards, reducing the speed of volume loss, while the outlet glaciers continued to retreat. Between 1928 and

1961, the ice thickness substantially decreased over the entire ice cap and the ice cap margin retreated everywhere along the outline of Hardangerjøkulen (Fig. 9). The modelled ice cap extent in 1961 corresponds quite well to the documented glacier outline for the south-western part of the ice cap; in the north-eastern part the modelled ice cap is too large (H. Elvehøy, personal communication, 2009). The period between 1961 and 1995 is characterized by steadily increasing net mass balances, culminating in the anomalously positive mass balance years in the late 1980s and early 1990s. An advance in the late 1990s is modelled for Midtdalsbreen, but not for Rembesdalsskåka, where the measured advance was significantly larger (Fig. 10). The length change measurements are however conducted at a different location than the end of the flowline we used to determine the glacier length of Rembesdalsskåka. The model underestimates the length change of Midtdalsbreen through the entire 20th century. When we choose a smaller initial ice cap geometry to simulate the 20th century evolution of Midtdalsbreen, the length record is better reproduced. Hence, even for a century-long simulation, the initial conditions are important for the final result.

We find that the coupled model is well able to reproduce the observed variations of Hardangerjøkulen through the 20th century. The model performs somewhat less for the north-eastern part of the ice cap, probably a result of the initial ice thickness or the precipitation distribution, which is more uncertain for this area.

5.7 Hardangerjøkulen in the 21st century

The effect of different climate scenarios on the modelled ice cap mass balance and volume and the length of Rembesdalsskåka and Midtdalsbreen is shown in Table 2. All absolute and relative changes are given for the year 2086 with respect to a reference run with the unchanged control climate. By our definition of the climate projection, the projected change in climate for 2071–2100 occurs in 2086. The modelled volume and length evolution through the 21st century are shown in Fig. 11 for a selection of the investigated climate scenarios.

When the climate is unchanged, i.e. when the control climate is prescribed, the net

mass balance is slightly positive and Hardangerjøkulen retains its present-day geometry. For increasingly positive temperature anomalies, the ice volume quickly decreases and Rembesdalsskåka and Midtdalsbreen retreat. For a temperature change of +3°C over the period 1976–2086, distributed equally over the year, Hardangerjøkulen has almost completely disappeared by the year 2100. It should be noted that the large jumps in the lengths of Rembesdalsskåka and Midtdalsbreen prior to their disappearance occur because the ice disappearing last from the basins is situated at a distance from the head of the present-day glacier.

Climate warming mainly affects the summer mass balance, but the winter balance also significantly decreases. A 10% precipitation increase along with the 3°C temperature increase has only a small effect on the projected volume and length changes. For a 50% precipitation increase, the ice cap disappears more slowly, but the effect of the temperature increase is by far not compensated. Even for a doubling of the precipitation (ΔP = +100%), which may compensate a 3°C warming according to the computed static mass balance sensitivities (Sect. 5.5), a significant reduction of Hardangerjøkulen's ice volume is projected for 2100. Apparently, non-linear effects associated with the much larger climate change than used to compute the mass balance sensitivities and the transient nature of the climate projections lead to more negative surface mass balances.

A seasonally varying change in air temperature and precipitation with the maximum change in autumn (15 October) does not lead to a notably different response of the ice cap (Table 2). However, when the maximum change occurs in winter (15 January), the winter balance remains more positive and the summer and net balance less negative, resulting in a slower decrease in ice volume and retreat of the outlet glaciers. Hence, the timing of the maximum change in temperature and precipitation does affect the mass balance and consequently the response of the glacier. The mass balance on Hardangerjøkulen is most sensitive to temperature changes in mid-summer and precipitation changes in late-autumn and early winter (Sect. 5.5). When the maximum temperature change occurs in winter, temperatures are still far too low to affect the

TCD
3, 947–993, 2009

snow accumulation or induce melt (Fig. 4). On the other hand, the smaller temperature increase from late spring to early autumn with respect to a constant annual change, leads to a higher winter balance and less summer ablation. Additional precipitation in winter further enhances this effect. For a maximum change in autumn, the mass balance is similar to the case without a seasonal cycle because opposite changes occur in spring and autumn, when the sensitivity to temperature and precipitation changes is similar.

An increase in the wind speed, simulated by a 10% increase in the turbulent exchange coefficient together with the 3°C temperature increase, has a negligible effect on the modelled response of Hardangerjøkulen ($\Delta V_{\mathrm{ice}} = -89\%$ in 2086, instead of −88%). A similarly prescribed cloud fraction increase of +0.05 also only slightly changes the model results ($\Delta V_{\mathrm{ice}} = -91\%$). Apparently, the effect of the temperature increase on the incoming longwave radiation and the turbulent fluxes is much larger than changes induced by an increase in cloudiness or wind speed.

For one of the most probable scenarios according to the RegClim results ($\Delta T = +3$°C and $\Delta P = +10\%$), we discuss the modelled future changes in more detail. In the very near future, by 2010, the equilibrium-line altitude (ELA) is expected to be situated around 1740 m a.s.l. and only 35% of the total ice cap is located above the ELA (Fig. 12). However, the 2010 ice cap (Fig. 13) is very similar to the ice cap modelled for 1995 (Fig. 9) and 2005, because the ice volume only just started to decrease after reaching a maximum in the year 2000 (Fig. 10). Between 2010 and 2040, the net mass balance becomes negative at all altitudes (Fig. 12a), implying that the entire ice cap is bound to disappear, even without increased future warming. A temperature change exceeding +1°C already positions the ELA above the ice cap; in this simulation this occurs around the year 2015. The largest mass balance changes are simulated at the higher altitudes, where the albedo changes most. In 2040, the outlet glaciers have retreated from the present-day margin and the ice thickness in the interior has approximately decreased by 50 m. A significant retreat occurs between 2040 and 2070, the ice cap plateau splits up into separate outlet glaciers and the ice thickness considerably

decreases (Fig. 13). Because the ice layer at the high bedrock ridges is relatively thin (<100 m, Fig. 9), it has completely melted away by 2070, while ice still remains at the lower altitudes where the ice is thicker. By 2100, almost all ice has disappeared, thin ice layers only remain in the basins where the present-day ice is thickest.

5.8 Feedback processes

The role of feedback processes in the response of Hardangerjøkulen was investigated by performing additional model simulations for $\Delta T = +3^{\circ}$C and $\Delta P = +10\%$ and excluding one process at a time.

To determine the effect of the mass balance–altitude feedback, the mass balance distribution was computed on the 2005 topography for all years. In the first years, the ice volume decrease is only slightly smaller when the mass balance-altitude feedback is excluded (Fig. 14), because the surface topography is still similar. By the year 2100, the ice volume difference has increased to almost 2 km^3 or 15% of the initial ice volume (2006).

Subsequently, we completely turned off ice flow to assess to what extent volume changes are determined by the local mass balance. Because the ice is no longer transported from high to low mass balance areas, thinning increases at the lower altitudes, while the change in ice thickness is reduced at the upper altitudes. As a result, the ice volume decreases more slowly than in the original simulation and attains almost exactly the same value in 2100 as in the simulation without mass balance–altitude feedback.

Hence, including ice flow and the mass balance–altitude feedback in a realistic way significantly speeds up the ice volume decrease. Nevertheless, in this case the mass balance changes projected for the future are so large that Hardangerjøkulen still rapidly disappears when these processes are not included.

6 Conclusions and discussion

A spatially distributed mass balance model was coupled to a two-dimensional ice-flow model to simulate the response of Hardangerjøkulen to projected climate change in the 21st century. By using a physically based mass balance model, projected changes in the meteorological variables could directly be incorporated in the model. Furthermore, the interactive coupling between the mass balance and ice-flow models ensured that feedback processes were included. The model was first validated with a simulation through the 20th century and was found to reproduce the evolution of Hardangerjøkulen as observed from changes in the glacier length and the surface topography.

For the projected 3°C warming, the model simulation indicated that Hardangerjøkulen will have almost disappeared by the end of the 21st century. The probable 10% increase in precipitation only slightly changed the modelled response; even a 100% precipitation increase could not fully compensate the effect of the temperature change. When the largest changes in temperature and precipitation were prescribed in winter, similar to the projections, the ice cap disappeared slower. However, none of the probable changes in the other meteorological variables had such a large effect as a 3°C warming.

Although we used a physically based model, there are still many factors adding uncertainty to the results. First of all, the future climate was modelled in a simple way. The interannual variability in the present-day climate of southern Norway is large, but we prescribed the same annual cycle for every year. Moreover, the projected climate change was assumed to be constant or seasonally varying, while changes will most likely not be the same for different weather types. Secondly, the mass balance model contains several parameterizations which may be different for the future climate and ice cap. One example is the ice albedo, which was assumed to be constant in space and time. In a warmer climate with less snowfall and a larger ablation area, more dust may accumulate on the ice surface, decreasing the albedo. A systematic lowering of the ice albedo has already been observed on Morteratschgletscher in Switzerland (Oerlemans

TCD
3, 947–993, 2009

et al., 2009). Still, lowering the ice albedo from 0.35 to 0.20 in the model simulation with $\Delta T = +3^{\circ}$C and $\Delta P = +10\%$, only lead to a 5% larger volume decrease. The precipitation distribution and the snowpack structure were also simulated in a simple way and may not be correct for a warmer climate and a different ice cap topography. A high-resolution atmospheric model and a sophisticated snowpack model are needed to improve the model in this respect, which is outside the scope of this study. Finally, increased meltwater production at the surface may enhance basal sliding and change the ice dynamics of Hardangerjøkulen. We expect that the warm, present-day ice cap already has an efficient drainage system and that this effect will therefore be small.

By using a coupled model where the terms in the surface energy and mass balance are computed individually, the effect of climate change on the mass balance and geometry of Hardangerjøkulen was included in a realistic way. The largest uncertainties in the model results can therefore be ascribed to the large range in climate scenarios and not to the model design. We can conclude that, provided that a 3°C warming indeed occurs in the 21st century and the precipitation increase is modest, Hardangerjøkulen is bound to disappear within the next 100 years.

The other maritime glaciers and ice caps in southern Norway have similar characteristics as Hardangerjøkulen and will probably also rapidly lose volume in the 21st century. A fast disappearance in a warmer climate has been projected for Nigardsbreen, an outlet glacier from the ice cap Jostedalsbreen, 130 km north of Hardangerjøkulen (Oerlemans, 1997). Although he uses a simple mass balance representation and a flowline model, the results are similar. Only a small warming rate is needed for a significant decrease in ice volume, a simultaneous increase in precipitation only delays the glacier retreat. The more continental glaciers further inland have a more regular hypsometry and are situated at higher altitudes. These glaciers are less sensitive to climate change and have a better chance to survive the 21st century, although largely reduced in size. Still, reconstructions of the Holocene glacier extent in southern Norway suggest that glaciers were absent in all glacierized regions during one or more periods in the early-/mid-Holocene, while air temperatures were probably lower than

TCD
3, 947–993, 2009

the temperatures projected for the end of the 21st century. Applying the coupled model to a number of well-studied glaciers in different regions could give a more definitive answer on the future of the glaciers in southern Norway.

Acknowledgements. We are grateful to Jojanneke van den Berg for providing the ice-flow model code and Kjetil Melvold for providing the ice thickness measurements and computing the ice thickness distribution for the entire ice cap. The Norwegian Meteorological Institute is acknowledged for access to and use of their meteorological database eKlima. We thank NVE, in particular Hallgeir Elvehøy, for providing the mass balance and length change measurements.

Appendix A Synoptic weather station data

A1 Local stations (1957–2005)

From 1957 onwards, digitized data from weather stations in the vicinity of Hardangerjøkulen are available from the Norwegian Meteorological Institute (NMI; see Fig. 1). Whenever possible, we used records from the nearest station, located north of Hardangerjøkulen. This station was relocated and renamed two times during the period considered, subsequently being called Slirå (1957–1969), Finse (1970–1993) and Finsevatn (1994–2005). Slirå and Finse were manned stations, Finsevatn is an automatic weather station. At Slirå, all necessary variables were measured. Air pressure was not measured at Finse, for which we use data from Voss. From Finsevatn we only use air temperature and air pressure measurements, the relative humidity and precipitation records contain large gaps and are unreliable. Cloudiness is not measured at Finsevatn. Precipitation is taken from measurements at Liset, which despite its location on almost the opposite side of Hardangerjøkulen as Slirå and Finse, has a very similar interannual variability in winter precipitation. For the overlap period 1974–1993, the correlation coefficient of annual November–March precipitation at Finse and Liset is 0.97. From 1994 onwards, we use relative humidity and cloud fraction observations from Eidfjord Bu. Compared to Slirå and Finse, Eidfjord Bu is located far from Hardan-

gerjøkulen. Still, for the overlapping period (1978–1994), the frequency distribution of cloud fractions at Eidfjord Bu and Finse is similar, the mean cloud fraction is equal and the cloud fraction records show simultaneous fluctuations. Air temperature measured at Eidfjord Bu is used to convert the relative humidity measurements to water vapour pressure. At Liset, precipitation is measured once a day at 06:00 UTC, at Slirå and Finse measurements were made at 06:00 and 18:00 UTC. The other variables are measured at 06:00, 12:00 and 18:00 UTC, sometimes measurements were made at 00:00 or 09:00 UTC as well. Hourly data are available for Finsevatn.

A2 Bergen (1904–2005)

Before 1957, the nearest synoptic station with available data is the NMI station in Bergen (Fig. 1), located approximately 120 km west of Hardangerjøkulen. We use records from 1904 onwards, when measurements were started at Bergen Fredriksberg, measurements from Bergen Florida are used from 1985 onwards. For the period 1904–1949, only measurements of air temperature, relative humidity and precipitation are available. After 1950, additional meteorological variables are available for Bergen, but we only use air temperature, relative humidity and precipitation for the entire period until 2005. In this way, the performance of the model with the limited data set from Bergen could be compared to results with the more extensive input data set from nearby weather stations. Air temperature and relative humidity are measured at 06:00, 12:00 and 18:00 UTC. For Bergen Florida measurements at 00:00 UTC are also available, the frequency increasing to 3-hourly data in 1996 and hourly data in 1998. Precipitation is measured twice a day (06:00 and 18:00 UTC).

A3 Implementation in the model

Since we use mass balance years instead of calendar years, the first model year starts at 1 October of the first year with available meteorological data. Hence, model runs are performed for the mass balance years 1958–2005 and 1905–2005 with the local and

Bergen input data sets, respectively.

When air temperature measurements were available for three-hour intervals, measurements were linearly interpolated to obtain hourly input data. For the data sets with three or four measurements per day, the daily cycle was approximated by a sine function fitted through the available measurements. Seasonally varying lapse rates for temperature are necessary to correct for differences in the boundary-layer structure at the meteorological station and the glacier surface (Giesen et al., 2009). Separate lapse rates were applied for the local and Bergen data, determined from the difference in monthly mean values between the input data and the AWS measurements on Midtdalsbreen for the period 2001–2005. Values range between 6.5 and 9.7 $\mathrm{K\,km^{-1}}$. Relative humidity measurements were linearly interpolated between measurement times to create an hourly input data set. Air pressure input data were not interpolated to obtain hourly values, we only calculate the air pressure field at the measurement times. For the model runs with data from Bergen, we prescribe a seasonally varying air pressure at the AWS altitude with a sine function, based on the AWS measurements. The cloud fraction input data were linearly interpolated between measurement times to create an hourly input data set. For runs with the Bergen data set, we prescribe the cloud fraction with a seasonally varying sinusoidal function derived from the AWS measurements. The daily precipitation sum from the input data is distributed evenly over the day in the model. As the measurement period at the NMI stations does not coincide with a calendar day, we prescribe the precipitation sum measured between 6 and 06:00 UTC the following day on the first day, hence the record is shifted 6 h backward. For each precipitation data set (Slirå, Finse, Liset and Bergen), we determined a multiplication constant to relate measured precipitation to accumulation at the ice cap by fitting modelled to measured annual winter balance on Rembesdalsskåka for all overlapping years. In this way, the total amount of winter accumulation is constrained to the measured winter balance, but interannual variations are preserved. Precipitation from Slirå and Finse is multiplied by 0.5 whenever the station temperature is above the threshold temperature for snow, to correct for overestimated values in summer resulting from

snow undercatch in winter.

References

Alley, R. B., Mayewski, P. A., Sowers, T., Stuiver, M., Taylor, K. C., and Clark, P. U.: Holocene climate instability: a prominent, widespread event 8200 yr ago, Geology, 6, 483–486, 1997. 951

Andersen, J. L. and Sollid, J. L.: Glacial chronology and glacial geomorphology in the marginal zones of the glaciers, Midtdalsbreen and Nigardsbreen, south Norway, Norsk Geogr. Tidssk., 25, 1–38, 1971. 951, 952, 965

Andreassen, L. M. and Elvehøy, H.: Volume change – Hardangerjøkulen, in: Glaciological investigations in Norway in 2000, edited by Kjøllmoen, B., NVE Report No 2, 101–102, Norwegian Water Resources and Energy Directorate, Oslo, 2001. 962

Andreassen, L. M., Elvehøy, H., Kjøllmoen, B., Engeset, R. V., and Haakensen, N.: Glacier mass-balance and length variation in Norway, Ann. Glaciol., 42, 317–325, 2005. 948, 949, 950, 951

Bahr, D. B., Dyurgerov, M., and Meier, M. F.: Sea-level rise from glaciers and ice caps: A lower bound, Geophys. Res. Lett., 36, doi:10.1029/2008GL036309, 2009. 948

Bjune, A. E., Bakke, J., Nesje, A., and Birks, H. J. B.: Holocene mean July temperature and winter precipitation in western Norway inferred from palynological and glaciological lake-sediment proxies, The Holocene, 15, 177–189, 2005. 951

Dahl, S. O. and Nesje, A.: Holocene glacier fluctuations at Hardangerjøkulen, central-southern Norway: a high-resolution composite chronology from lacustrine and terrestrial deposits, The Holocene, 4, 269–277, 1994. 951

De Woul, M. and Hock, R.: Static mass-balance sensitivity of Arctic glaciers and ice caps using a degree-day approach, Ann. Glaciol., 42, 217–224, 2005. 964

Elvehøy, H., Kohler, J., Engeset, R., and Andreassen, L. M.: Jøkullaup fra Demmevatn, NVE Report No 17, Norwegian Water Resources and Energy Directorate, Oslo, 36 pp., 1997. 951, 952

Fægri, K.: Forandringer ved norske breer 1934–35, Bergen Museums Årbok 1935, Naturvidenskapelig rekke Nr. 6, Bergen, Norway, 10 pp., 1936. 965

Giesen, R. H.: The ice cap Hardangerjøkulen in the past, present and future climate, Ph.D. the-

sis, Institute for Marine and Atmospheric research Utrecht, Utrecht University, The Netherlands, available at http://www.phys.uu.nl/~giesen, 2009. 952, 953, 965
Giesen, R. H., van den Broeke, M. R., Oerlemans, J., and Andreassen, L. M.: The surface energy balance in the ablation zone of Midtdalsbreen, a glacier in southern Norway: Interannual variability and the effect of clouds, J. Geophys. Res., 113, doi:10.1029/2008JD010390, 2008. 951, 957, 961
Giesen, R. H., Andreassen, L. M., van den Broeke, M. R., and Oerlemans, J.: Comparison of the meteorology and surface energy balance at Storbreen and Midtdalsbreen, two glaciers in southern Norway, The Cryosphere, 3, 57–74, 2009, http://www.the-cryosphere-discuss.net/3/57/2009/. 949, 974
Hutter, K.: Theoretical glaciology : material science of ice and the mechanics of glaciers and ice sheets, Reidel, Dordrecht, The Netherlands, 1983. 952
Huybrechts, P.: The Antarctic ice sheet and environmental change: a three-dimensional modelling study, Reports on polar research, 99, 241 pp., 1992. 952
IPCC: Climate Change 2007: The Physical Science Basis. Contribution of Working Group I to the Fourth Assessment Report of the Intergovernmental Panel on Climate Change [Solomon, S., D. Qin, M. Manning, Z. Chen, M. Marquis, K.B. Averyt, M. Tignor and H.L. Miller (eds.)], Cambridge University Press, Cambridge, United Kingdom and New York, NY, USA, 2007. 948
Kjøllmoen, B., Andreassen, L. M., Engeset, R. V., Elvehøy, H., Jackson, M., and Giesen, R. H.: Glaciological investigations in Norway in 2005, NVE Report No 2, Norwegian Water Resources and Energy Directorate, Oslo, 91 pp. +app., 2006. 950
Kjøllmoen, B., Andreassen, L. M., Elvehøy, H., Jackson, M., Giesen, R. H., and Winkler, S.: Glaciological investigations in Norway in 2007, NVE Report No 3, Norwegian Water Resources and Energy Directorate, Oslo, 91 pp., 2008. 949
Klok, E. J. and Oerlemans, J.: Model study of the spatial distribution of the energy and mass balance of Morteratschgletscher, Switzerland, J. Glaciol., 48, 505–518, 2002. 953
Laumann, T.: Snø, firn, is – en undersøkelse på Hardangerjøkulen, Master's thesis, University of Oslo, 1972. 954
Leysinger Vieli, G. J.-M. C. and Gudmundsson, G. H.: On estimating length fluctuations of glaciers caused by changes in climatic forcing, J. Geophys. Res., 109, doi:10.1029/2003JF000027, 2004. 952
Liestøl, O.: Glacier dammed lakes in Norway, Norsk Geogr. Tidssk., 15, 122–149, 1956. 965

Meier, M. F., Dyurgerov, M. B., Rick, U. K., O'Neel, S., Pfeffer, W. T., Anderson, R. S., Anderson, S. P., and Glazovsky, A. F.: Glaciers dominate eustatic sea-level rise in the 21st century, Science, 317, 1064–1067, doi:10.1126/science.1143906, 2007. 948

Nesje, A. and Dahl, S. O.: Holocene glacier variations of Blåisen, Hardangerjøkulen, central southern Norway, Quaternary Res., 35, 25–40, 1991. 951

Nesje, A., Dahl, S. O., Løvlie, R., and Sulebak, J. R.: Holocene glacier activity at the southwestern part of Hardangerjøkulen, central-southern Norway: evidence from lacustrine sediments, The Holocene, 4, 377–382, 1994. 951

Nesje, A., Bakke, J., Dahl, S. O., Lie, Ø., and Matthews, J. A.: Norwegian mountain glaciers in the past, present and future, Global Planet. Change, 60, 10–27, 2008. 949, 951

Oerlemans, J.: A flowline model for Nigardsbreen, Norway: projection of future glacier length based on dynamic calibration with the historic record, Ann. Glaciol., 24, 382–389, 1997. 952, 971

Oerlemans, J.: Glaciers and Climate Change, Balkema, Lisse, 2001. 953, 963

Oerlemans, J. and Reichert, B. K.: Relating glacier mass balance to meteorological data by using a seasonal sensitivity characteristic, J. Glaciol., 46, 1–6, 2000. 964

Oerlemans, J., Giesen, R. H., and van den Broeke, M. R.: Retreating alpine glaciers: increased melt rates due to accumulation of dust (Vadret da Morteratsch, Switzerland), J. Glaciol., 55, 729–736, 2009. 970

Räisänen, J., Hansson, U., Ullerstig, A., Döscher, R., Graham, L. P., Jones, C., Meier, H. E. M., Samuelsson, P., and Willén, U.: European climate in the late twenty-first century: regional simulations with two driving global models and two forcing scenarios, Clim. Dyn., 22, 13–31, 2004. 957

Rasmussen, L. A. and Conway, H.: Influence of upper-air conditions on glaciers in Scandinavia, Ann. Glaciol., 42, 402–408, 2005. 964

Van den Berg, J., van de Wal, R. S. W., and Oerlemans, J.: A mass balance model for the Eurasian Ice Sheet for the last 120,000 years, Global Planet. Change, 61, 194–208, 2008. 952

Table 1. Linear correlation coefficient r and the mean difference between modelled and measured winter, summer and net mass balance ΔB (mw.e.) for Rembesdalsskåka over the period 1963–2005.

	winter		summer		net	
	r	ΔB	r	ΔB	r	ΔB
Local, z_s DEM	0.92	−0.06	0.75	+0.05	0.88	−0.01
Local, z_s model	0.91	−0.05	0.75	+0.04	0.88	−0.01
Bergen, z_s DEM	0.82	−0.04	0.74	+0.19	0.85	+0.15
Bergen, z_s model	0.81	−0.01	0.75	+0.19	0.85	+0.18

TCD
3, 947–993, 2009

Table 2. Effect of different changes in air temperature (ΔT) and precipitation (ΔP) on the modelled winter (B_w), summer (B_s) and net (B_n) surface mass balance and ice volume (V_{ice}) of Hardangerjøkulen and the length of Rembesdalsskåka (L_{Remb}) and Midtdalsbreen (L_{Midt}) in the year 2086. The climate projections are prescribed as an annual and as a seasonally varying change, with the maximum on either 15 October or 15 January. All changes (Δ) are given with respect to the reference run with the control climate for 1961–1990. The surface mass balance is the total surface mass balance over the modelled ice cap.

	ΔT (°C)	ΔP (%)	B_w (mw.e.)	B_s (mw.e.)	B_n (mw.e.)	V_{ice} (km^3)	L_{Remb} (km)	L_{Midt} (km)
Reference	0	0	+2.03	−1.95	+0.08	12.1	9.1	4.9
			ΔB_w (mw.e.)	ΔB_s (mw.e.)	ΔB_n (mw.e.)	ΔV_{ice} (%)	ΔL_{Remb} (%)	ΔL_{Midt} (%)
Annual	+1	0	−0.12	−0.83	−0.96	−31	−5	−14
Annual	+2	0	−0.45	−2.30	−2.75	−64	−22	−37
Annual	+3	0	−0.96	−3.53	−4.50	−88	−27	−51
Annual	+4	0	−1.52	−4.76	−6.28	−97	−42	−100
Annual	+3	+10	−0.71	−3.39	−4.10	−84	−25	−49
Annual	+3	+50	+0.32	−2.93	−2.61	−60	−21	−23
Annual	+3	+100	+1.60	−2.36	−0.76	−14	−2	−12
Seasonal, max. 15 Oct	+3	0	−0.98	−3.56	−4.54	−89	−27	−55
Seasonal, max. 15 Oct	+3	+10	−0.68	−3.41	−4.08	−84	−25	−49
Seasonal, max. 15 Jan	+3	0	−0.79	−3.02	−3.81	−81	−25	−47
Seasonal, max. 15 Jan	+3	+10	−0.33	−2.79	−3.12	−70	−23	−39

TCD
3, 947–993, 2009

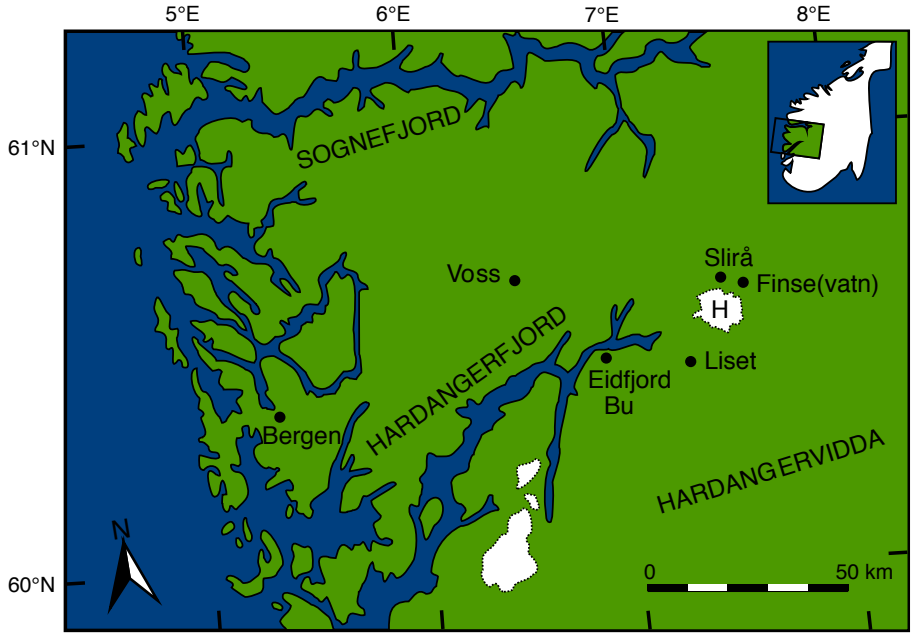

Fig. 1. Map showing the location of Hardangerjøkulen (H) in southern Norway and the locations of the synoptic weather stations from which records are used in this study.

TCD
3, 947–993, 2009

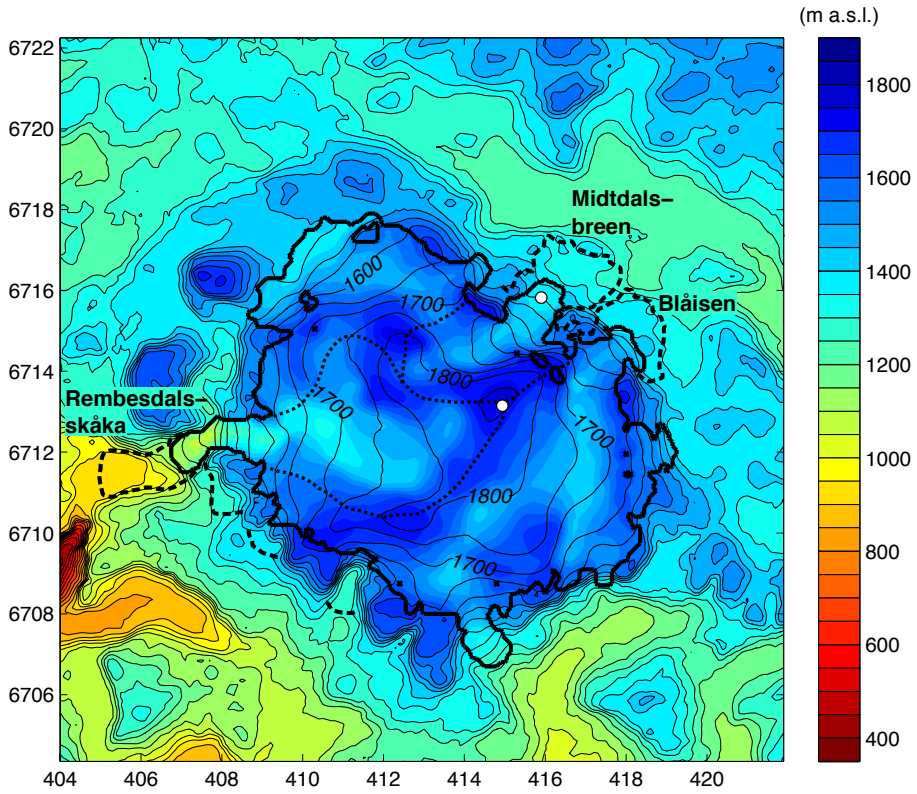

Fig. 2. Present-day surface topography (contours) and bedrock topography (colouring) in the model domain, contours are drawn every 50 m. The thick solid line indicates the present-day ice cap extent, the thick dashed lines the reconstructed Little Ice Age extent (references in text) and the dotted lines the drainage basins of Rembesdalsskåka and Midtdalsbreen. The locations of the AWSs on Midtdalsbreen and the ice cap summit are indicated by white dots. The reference system is UTM zone 32 (EUREF89), the tick mark spacing is 2 km.

TCD
3, 947–993, 2009

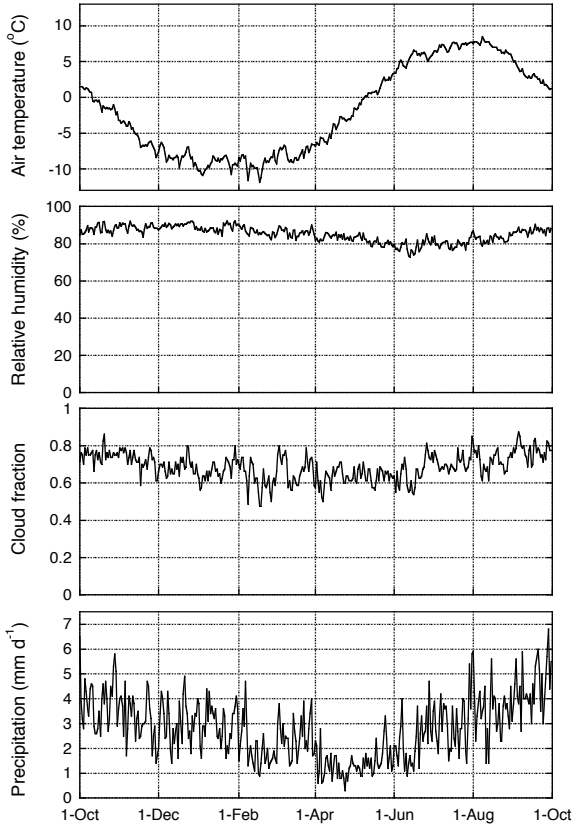

Fig. 3. Average seasonal cycle of meteorological variables over the period 1961–1990, used as the control climate for climate projections from 1961–1990 to 2071–2100. The curves show daily mean values.

TCD
3, 947–993, 2009

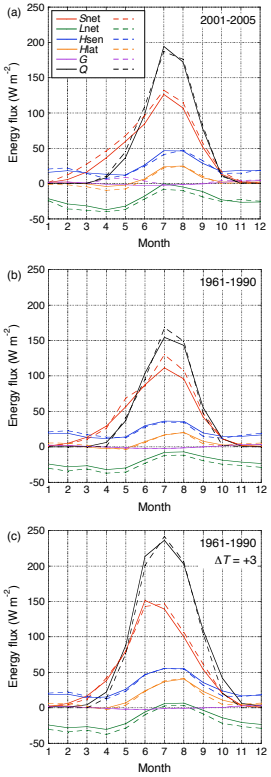

Fig. 4. Seasonal cycle of the surface energy fluxes at the AWS location on Midtdalsbreen, modelled with the local meteorological records (solid lines) for **(a)** 2001–2005, **(b)** 1961–1990 and **(c)** 1961–1990 with $\Delta T = +3^{\circ}$C. The dashed lines in (a) show the mean seasonal cycle of the AWS measurements for the same period, in (b) and (c) they show the results of similar runs with the control climate.

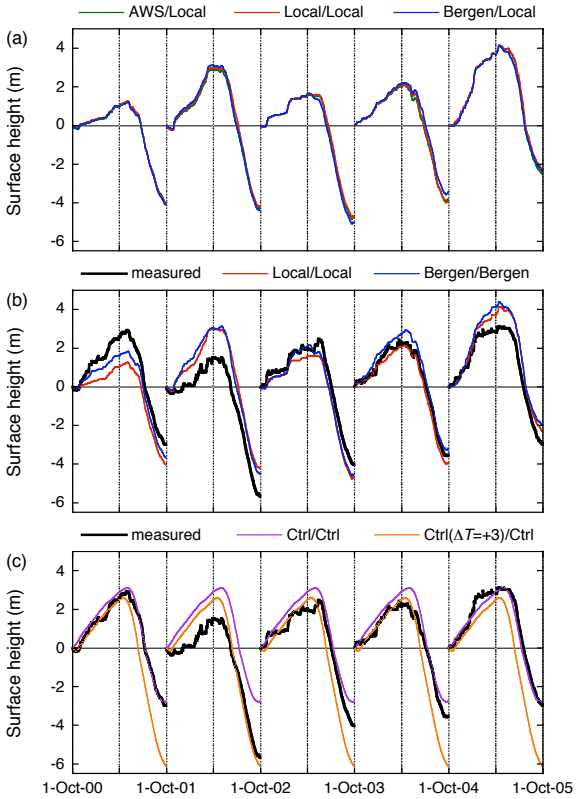

Fig. 5. Modelled surface height at the AWS location on Midtdalsbreen with **(a)** variable "meteo" (air temperature, humidity, pressure and cloudiness) records and local precipitation, **(b)** both the "meteo" and precipitation records from the two data sets, and **(c)** the control climate (Ctrl) and the control climate with a 3°C higher temperature, shown together with the measured surface height. The labels indicate the records used for the "meteo" and precipitation input in the order 'meteo'/precipitation.

TCD
3, 947–993, 2009

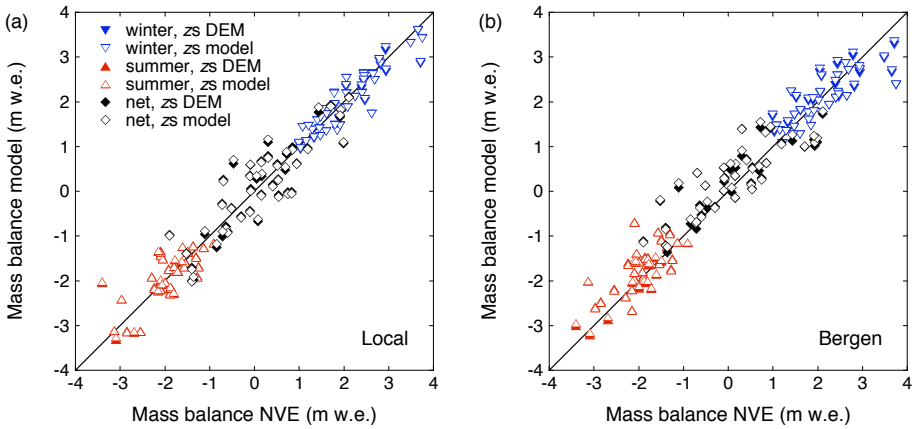

Fig. 6. Basin-averaged measured (NVE) and modelled winter, summer and net mass balance for Rembesdalsskåka for all 43 years in the period 1963–2005, using the two input data sets. Mass balances were calculated for a fixed topography (z_s DEM) and the modelled topography from the 20th century run (z_s model).

TCD
3, 947–993, 2009

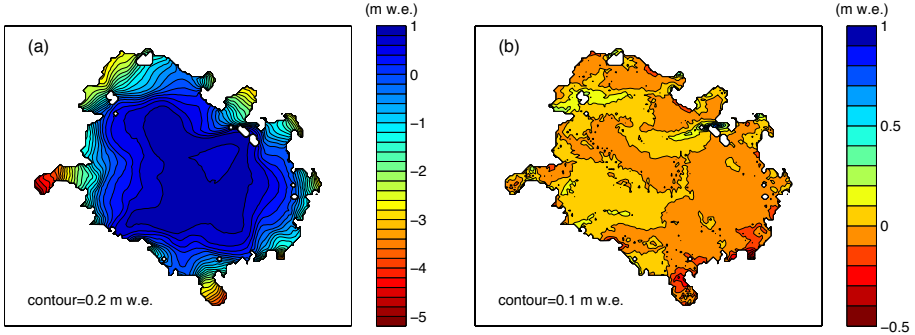

Fig. 7. (a) Mean and **(b)** altitudinal deviation of the net mass balance distribution for the period 1961–1990, modelled with local meteorological data.

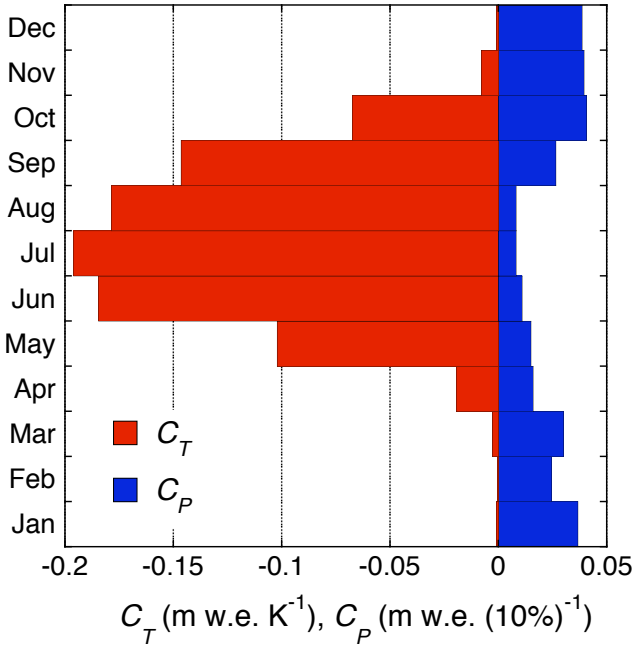

Fig. 8. Seasonal sensitivity characteristic of Hardangerjøkulen, showing the mass balance sensitivity to monthly perturbations in local air temperature and precipitation for the period 1961–1990. The monthly values were normalized to a period of 30 days.

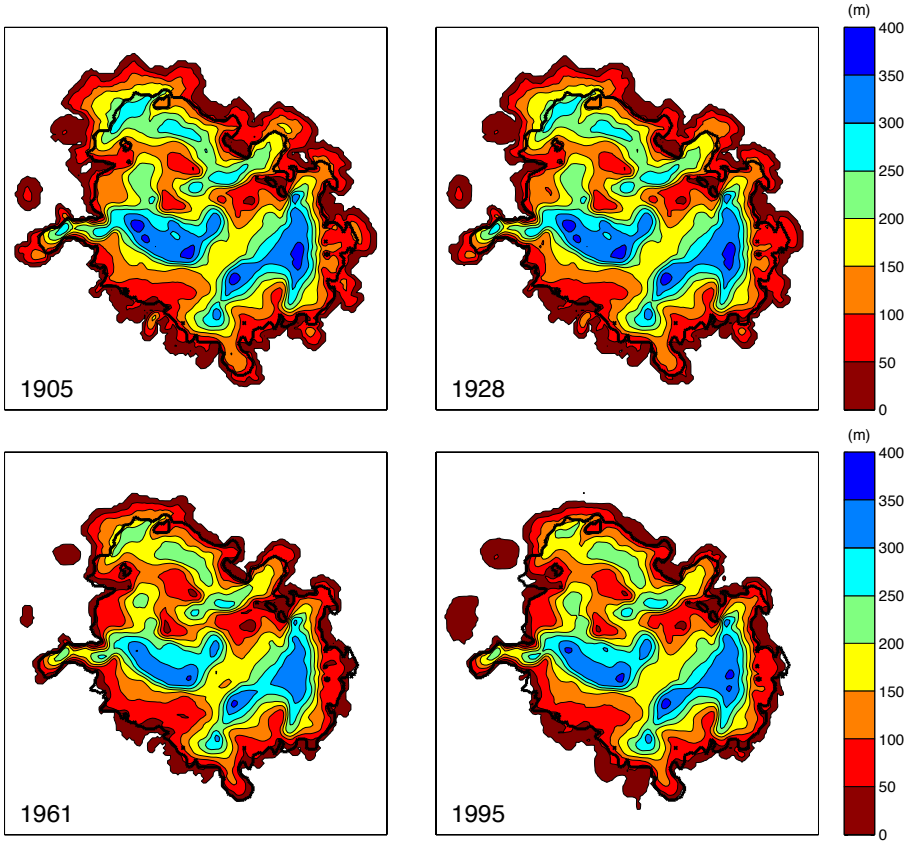

Fig. 9. Modelled ice thickness for 1905, 1928, 1961 and 1995. Contour lines are drawn for 50 m intervals. The thick line indicates the present-day ice cap outline.

TCD
3, 947–993, 2009

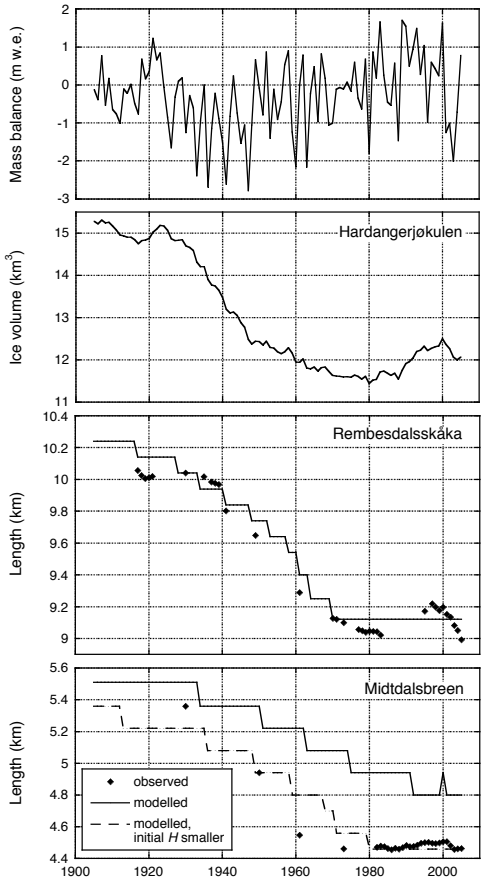

Fig. 10. Modelled net mass balance and ice volume for the entire ice cap and observed and simulated frontal variations at Rembesdalsskåka and Midtdalsbreen for the period 1905–2005. For Midtdalsbreen, an additional simulation starting from a smaller initial ice thickness is shown.

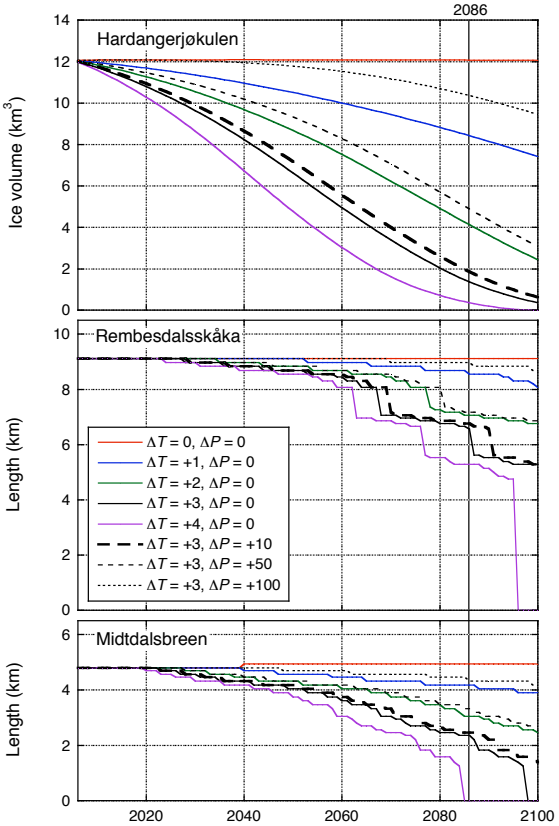

Fig. 11. Ice cap volume and length change for Rembesdalsskåka and Midtdalsbreen from 1905 to 2100 for different climate scenarios applied from 2006 onwards. The imposed temperature (ΔT in $^\circ$C) and precipitation (ΔP in %) changes are constant through the year.

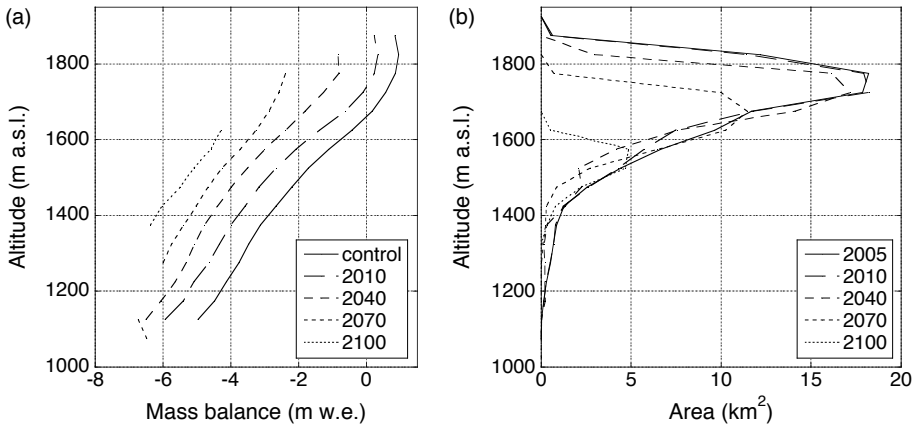

Fig. 12. Modelled (a) net mass balance profile and (b) area distribution for 2010, 2040, 2070 and 2100, for the climate projection with $\Delta T = +3^{\circ}$C and $\Delta P = +10\%$. The mass balance profile for the control climate and the area distribution at the end of 2005 are shown for reference.

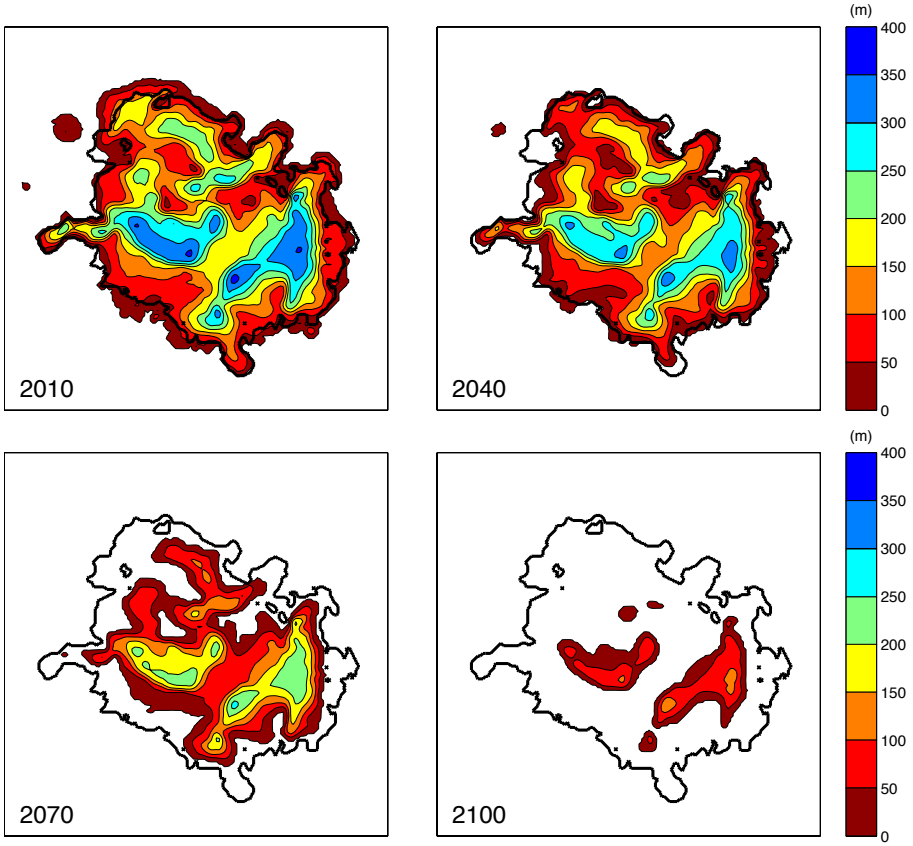

Fig. 13. Modelled ice thickness for 2010, 2040, 2070 and 2100, for the climate projection with $\Delta T = +3^{\circ}$C and $\Delta P = +10\%$. Contour lines are drawn every 50 m. The thick line indicates the present-day ice cap margin.

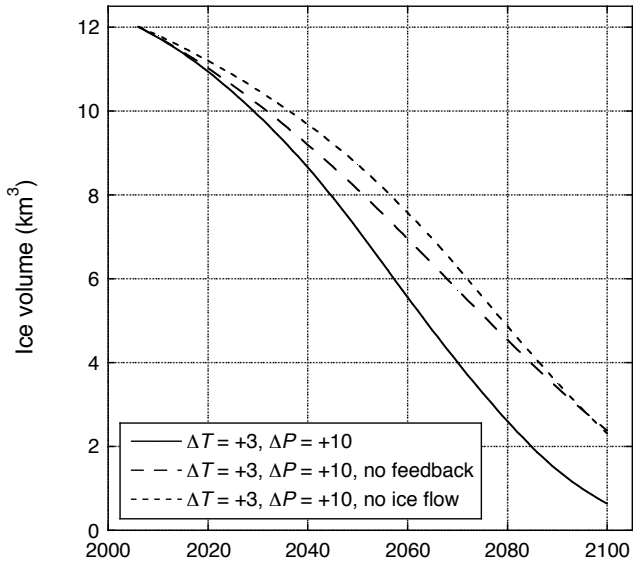

Fig. 14. Modelled ice cap volume from 2006 to 2100 for the climate projection with ΔT = +3°C and ΔP = +10%, shown together with simulations without the mass balance–altitude feedback and without ice flow.